Carbothermal synthesis of activated carbon-supported nano zero valent iron: effects of temperature, characterization, and reactivity

Wei-fang Chen[a,*], Chang-cheng Yan[a], Qiong Wang[a], Ling Pan[a], Li-fang Chen[b]

[a]*School of Environment and Architecture, University of Shanghai for Science and Technology, Shanghai 200093, China,*
Tel. +86 15026671846; Fax: +86 21 55275979; email: chenzjzj@gmail.com (W.-f. Chen), Tel./Fax: +86 21 55275979;
email: ycc1992@126.com (C.-c. Yan), Tel. +86 21 55270697; Fax: +86 21 55275979; emails: wangqiong@usst.edu.cn (Q. Wang),
linpan19@usst.edu.cn (L. Pan)
[b]*College of Marine Science and Engineering, School of Tianjin University of Science and Technology, Tianjin 300457, China,*
Tel. +86 18622431118; Fax: +86 22 62574210; email: chenlifang65@tust.edu.cn

ABSTRACT

Activated carbon-supported nano zero valent iron was synthesized through a carbonthermal reduction process. Specifically, iron-impregnated activated carbon was thermally treated under N_2 atmosphere at temperatures ranging from 350 to 1,150°C. Major properties of the synthesized materials were obtained through analysis of iron content, BET surface area, and pore size distribution. TEM images, X-ray diffraction (XRD), and Fourier transform infrared patterns were also obtained for characterization. Results show that zero valent iron was reduced from iron oxide and those nanoparticles were highly dispersed based on TEM images while XRD patterns indicate a progressive reduction of iron oxide to form elemental iron. Treatment temperature greatly impacted the characteristics of the carbonthermal products. The size of the particles, content of elemental iron, surface functional groups, and pore structure all changed with the change in treatment temperature. Synthesized materials were tested for their reactivities on chromate. Reduction of Cr(VI) by carbothermal products occurred based on analysis of Cr speciation. In addition, reduction ability differed with various carbothermal temperatures. Overall, materials synthesized at 550–750°C appears to stand out when chromate removal capability and removal rate are concerned.

Keywords: Carbothermal synthesis; Elemental iron; Activated carbon; Characterization; Chromate

1. Introduction

Nano zero valent iron (NZVI) has been successfully used in environmental remediation for halogenated compounds, hydrocarbons, nitrate, perchlorate, and toxic heavy metals [1]. Reduction by zero valent iron was considered to be the main pathway during remediation of pollutants such as halogenated aromatics and metal ions. However, nano iron is poor in mobility in porous media such as soil and groundwater aquifer [2]. Control of aggregation and optimizing of reactivity and stability are also issues stopping nano iron from realizing its full potential. In the last decade, studies in the field of nano iron have been mainly focused on solving these problems (aggregation,

*Corresponding author.

mobility, stability, etc.) [3]. Aggregation of NZVI was alleviated significantly by surface coating with anionic polyelectrolytes such as polyacrylic acid [4]. Nevertheless, transport of coated NZVI is still affected by surface charge heterogeneities encountered in aquifer. Application of electrokinetics was proposed by Chowdhury et al. to enhance NZVI transport in the subsurface, particularly through fine grained porous media when increasing advective transport of NZVI is impractical [5]. Studies have also revealed that carboxymethyl cellulose, polystyrene sulfonate, triblock copolymer, xanthan gum, or emulsion stabilized NZVI through electrostatic repulsion, steric hindrance, and depletion [6–8]. These coating materials were used as "delivery vehicles" to improve NZVI transporting. However, coatings of NZVI are unlikely to provide complete stabilization because of incomplete or insufficient surface coverage. In addition, the extent of stabilization is dependent on the characteristics of the coating materials, the thickness of the polymer layer on the particle surface, and the solution chemistry [9,10].

Supporting NZVI on porous materials such as silica [11], resin [12], montmorillonite [13], activated carbon [14], carbon nanotube [15], and zeolite [16] were reported to considerably reduce particle aggregation and increase the homogeneous dispersion of NZVI. Particles synthesized using a supporting material as matrix tend to exhibit a narrower size distribution. Most of nano iron-supported materials were made by chemical reduction by sodium borohydride of preloaded iron salts [17,18]. Scaling up is an issue with this chemical reduction method due to the production of hydrogen gas and the high chemical cost [19]. Thermal treatment has been considered an alternative process for NZVI synthesis. Carbothermal reduction is widely used in the production of iron and steel from iron ore. Carbon acted as the reductive agent. Hoch et al. prepared carbon black-supported NZVI by aqueous impregnation of iron salt and subsequent heat treatment at 600–800°C under argon [20]. At treatment temperature between 300 and 500°C, Fe_3O_4 was formed from adsorbed iron ions. Elemental iron appeared only in samples treated at higher than 600°C. Using an aerosol-based technology, Zhan et al. produced a carbon–iron composite from sucrose–iron salt mixture by a combination of hydrothermal dehydration and carbothermal reduction processes [21]. Pereira et al. obtained a magnetite-coated NZVI and activated carbon composite by the reduction of ferric nitrate-impregnated activated carbon in an inert gas atmosphere at up to 800°C [22]. These materials were found to be highly efficient in a variety of environmental applications, e.g. degradation of textile dye and reduction of Cr(VI) in aqueous medium.

This paper intended to investigate the production of activated carbon-supported NZVI particles through carbothermal treatment of activated carbon impregnated with iron. The effects of treatment temperature on carbothermal reduction, immobilization, and development of elemental iron were studied in detail. Besides providing element carbon as reducing agent, activated carbon showed other advantages due to its large surface area and sophisticated pore structure [23]. A variety of tools were employed to characterize the association between activated carbon and iron particles and to provide further information on the role of activated carbon.

In addition, chromate was employed as a target pollutant to investigate the reactivity of synthesized materials. Effects of dosage, mechanism, and rate of Cr removal and role of nano iron were investigated. The ultimate goal of this research is to optimize carbothermal synthesis condition and provide useful information on application through testing the efficiency for chromate removal.

2. Materials and methods

2.1. Materials

Lignite-based activated carbon purchased from Sinopharm Group Chemical Reagent, China was ground to 180×200 US mesh in size before use and named as AC. Potassium dichromate and iron(II) chloride tetrahydrate ($FeCl_2 \cdot 4H_2O$) were purchased from Aladdin, China. All chemicals were analytical grade and were used as received without further purification.

2.2. Carbothermal synthesis of activated carbon–nanoiron composites

Eight grams of activated carbon were dispersed into 200 mL of $FeCl_2$ (1 mol/L) solution and shaken at 120 rpm, 25°C for 24 h. The mixture was then put in an evaporator at 100°C until dry. Thus, iron-loaded sample was named as AC-Fe.

For carbothermal treatment, 4 g of AC-Fe was put in a tube furnace (XD1600, Zhenzhou Tianzong Electrical Equipment Co., Ltd, China) under N_2 atmosphere. Furnace temperature was ramped up to 350, 550, 750, 950, and 1,150°C, respectively, at 5°C/min and held for 2 h. After that, furnace was cooled down to room temperature and the resultant samples were washed thoroughly with ethanol and stored in a N_2-purged desiccator. Samples were named as AC-Fe-temperature. For instance, AC-Fe-350 is the sample treated at 350°C.

2.3. Effect of dosage on Cr removal

Activated carbon sample, 0.01, 0.05, 0.1, 0.15, 0.20, 0.30, or 0.40 g in mass, was added to flasks each containing 50 mL of dichromate solution (40 mg/L as Cr). All flasks were put on a shaker (120 rpm) at 25°C for 24 h. The suspension was then filtered through a 0.45 μm membrane filter. Filtrate was analyzed for total Cr.

$$Cr\ removal\ (\%) = \frac{C_0 - C}{C_0} \times 100\% \tag{1}$$

where C_0 is the initial Cr concentration and C is the residual Cr. pH of the solution was kept constant at around 5.7.

2.4. Effect of contact time on Cr removal

0.1 g of sample was added to eight flasks each containing 50 mL of 40 mg/L (as Cr) dichromate solution. pH was kept constant at around 5.7. The mixture was filtered after 10, 20, 30 min, 1, 2, 4, 8, 24, or 48 h of contact, and filtrate was analyzed for total Cr.

2.5. Material characterization and chemical analysis

X-ray powder diffraction was performed with a D8A A25 (Bruker Axs GMBH) using CuKα radiation at a scanning rate of 3°/min in the 2θ range from 20° to 80°. High Resolution Transmission Electron Microscope HR-TEM Tecnai G20 (FEI, USA) was used to observe the morphology and size of the composites. Infrared spectra of materials were obtained by a Fourier transform infrared spectrometer (FTIR) Magna-IR 750 (Nicolet, USA). Surface area and pore size distribution were determined by nitrogen adsorption–desorption isotherms by a 3H-2000PS4 unit (Beishide Instrument, China).

Cr(VI) was determined using a UV–vis spectrophotometer (723 N, Shanghai Jingke Industrial Co., Ltd) by the diphenylcarbazide colorimetric method. Total Cr was determined using atomic absorption spectrometry (TAS-990, PGENERAL Shanghai). Cr(III) concentration was calculated as the difference between total Cr and Cr(VI).

Ion content of samples was determined through a digestion method. 0.1 g of sample was added to 30 mL of HCl (3 mol/L) solution for 4 h at room temperature. The mixture was then filtered, and filtrate was analyzed for iron using atomic adsorption spectrometry. Cr speciation on solid surface was analyzed using the same digestion method.

3. Results and discussion

3.1. Physicochemical properties of synthesized materials

Fig. 1 is the iron contents of original activated carbon, AC-Fe, and carbothermally synthesized samples. There is about 0.39 mg/g iron with the original activated carbon stemming probably from raw material. After iron loading, iron content of AC-Fe rose to 18.24 mg/g. Iron content of thermally treated samples (AC-Fe-350 to AC-Fe-1150) ranged from 8.59 to 17.23 mg/g. After thermal treatment, samples were washed thoroughly with ethanol to remove loose iron particles. This may be the reason that iron content for thermally treated samples was less than AC-Fe. However, for thermally treated samples, iron content increased with the increase in treatment temperature. This may be due to the calcinations effect. Mackenzie et al. [24] reported that calcination increased the mechanical stability of nano iron on supporting material. With high temperature calcination, a greater portion of iron became stable on activated carbon surface.

Thermal treatment also led to the dispersion of iron particles as shown by the TEM images in Fig. 2. The large gray sheet is activated carbon while metal particles are shown as darker clusters. At 350°C, crystallites in the size of 10 nm were immobilized at the activated carbon surface. TEM images revealed that with the increase in temperature, iron became increasingly dispersed on activated carbon and was only a few nanometers in size for sample synthesized at temperatures higher than 750°C.

Physicochemical properties of AC-Fe and thermally treated samples were further recorded with X-ray diffraction (XRD) and FTIR.

Fig. 3 is the XRD patterns for activated carbon, AC-Fe, and carbothermally synthesized samples. The broad peak at around 26° was attributed to graphite-like
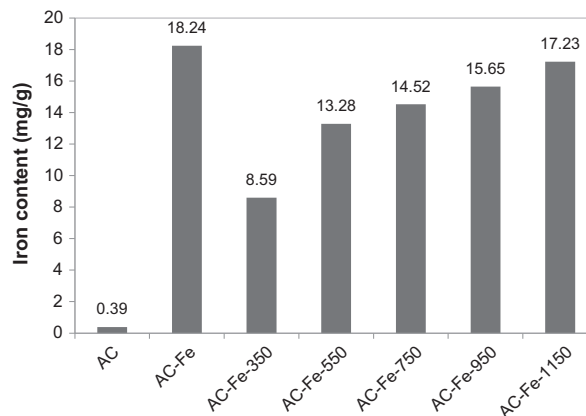
Fig. 1. Iron contents of original AC, AC-Fe, and carbothermally synthesized sample.
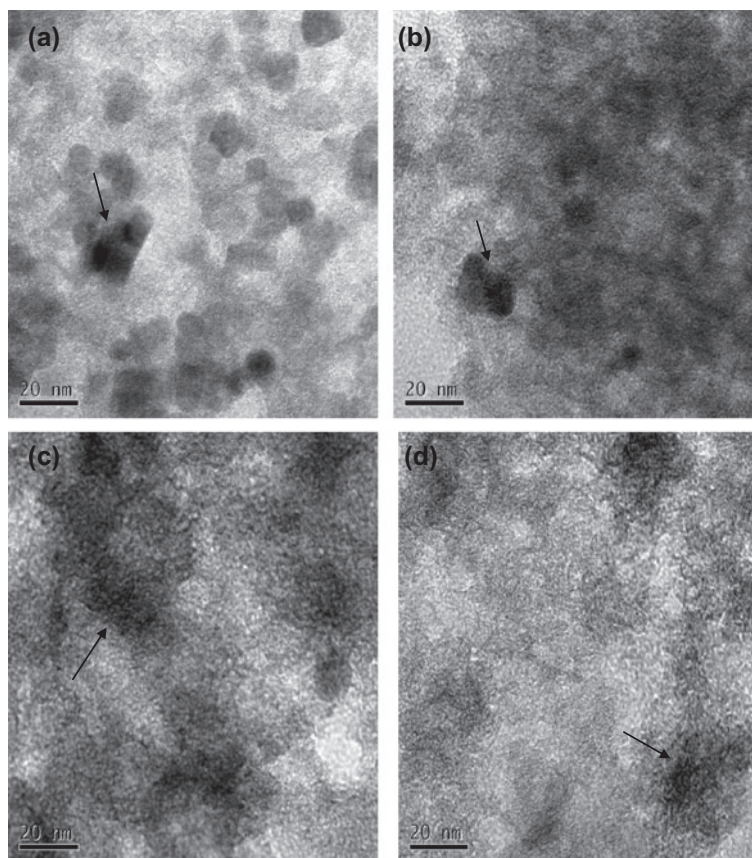
Fig. 2. TEM images of (a) AC-Fe-350; (b) AC-Fe-550; (c) AC-Fe-750; (d) AC-Fe-950.

reflection of activated carbon. No obvious peak of crystallite was observed with AC. For AC-Fe, only very small peak of magnetite crystallite at about 35° was present. Magnetite peak was strengthened with AC-Fe-350 indicating increasing conversion of preloaded iron ions or salts to Fe_3O_4 particles [25]. The peaks at 43–45° (Fe110) and 64.9° (Fe200) correspond to the elemental iron with a body-centered crystalline structure [26]. Between 500 and 900°C, magnetite peaks gradually disappeared and were replaced by peaks representing elemental iron. Very little of the oxide phase remained at temperature above 750°C. The progression in XRD patterns suggests that elemental iron is the product of carbothermal reduction of iron oxide. However, magnetite peaks reappeared for samples treated at 1,150°C (AC-Fe-1150). It is most likely that zero valent iron reacted with oxygen in air during sample handling. Compared to samples prepared at lower temperature (500–900°C), AC-Fe-1150 seems to be most reactive in air.

Fig. 4 displays a comparison of FTIR spectra with AC-Fe and carbothermally synthesized samples. Broad bands at around 3,400 cm^{-1} were attributed to O–H stretching, due to H_2O or C–OH. There are two prominent peaks 3,030 and 2,930 cm^{-1} that are indication of symmetric and asymmetric CH_2 vibration, respectively [27]. Bands at 1,620 and 1,130 cm^{-1} are presumed to be C=C and aliphatic C–H, respectively [28]. The most obvious changes between AC and AC-Fe samples in FTIR occur at bands observed around 702 cm^{-1}. These are Fe–O vibrations probably due in part from FeOOH layer on Fe^0 nanoparticles. Thermally treated samples showed much higher peaks of iron oxides.

In addition, changes in surface area and pore volume after carbothermal treatment were also compared. Table 1 is the BET surface area and pore volume. Fig. 5 is the pore size distribution. Compared with AC, surface area, total pore volume, and micropore volume all decreased after iron particles were deposited on activated carbon. The most obvious decrease occurred with pores in the size of 2–5 nm as shown in Fig. 5 when compared to original activated carbon. Iron oxides or elemental iron was dispersed in the original pore structure and led to the decline.

However, surface area and pore volume varied at different treatment temperatures. As temperature
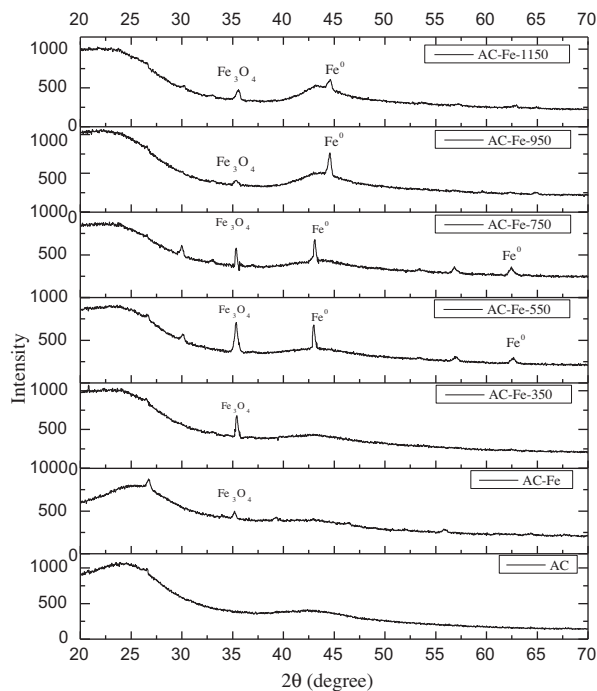
Fig. 3. XRD patterns of original AC, AC-Fe, and carbothermally synthesized samples.

Fig. 4. FTIR spectra of original AC, AC-Fe, and carbothermally synthesized samples.

increased from 350 to 550°C, surface area and pore volume increased. This may be due to the activation by iron compounds which could open up pores. Su et al. reported that iron compounds greatly facilitated the activation of coir pith, and micropores were formed at temperature 500–600°C [29]. In their research, both surface area and pore volume declined as temperature increased beyond 750°C. They argued that at high temperature sintering effect predominated and newly created pores were closed. In our research, the average pore size (last column in Table 1) dropped after temperature reached beyond 750°C, which is accompanied by the decreases in both total pore volume and micropore volume. This may mean that the decrease in pore size is most likely a result of pore closure rather than creation of micropores. The same sintering effect may be at work here. This effect is most obvious for AC-Fe-1150 which showed the lowest total pore volume and micropore volume.

Overall, from characterization, elemental iron was successfully created and dispersed on activate carbon surface. The morphology, surface structure of original activated carbon was changed with the depositing of nanoparticles.

3.2. Effect of dosage on Cr removal

Reactivity of carbothermally synthesized materials was investigated with chromate as the target substrate. Cr removal by activated carbon, iron-loaded activated carbon AC-Fe was also carried out for comparison. Fig. 6 is the effect of dosage on total Cr removal. AC had limited adsorption capacity for Cr. Dosage increased from 0.2 to 8.0 g/L, percentage of Cr removal changed from 12.2 to 55.2%. AC-Fe showed strong removal for Cr. More than 80% of the initial Cr was removed at dosage >6 g/L. According to XRD patterns, iron oxides were formed on AC-Fe surface. Luo et al. [30] believed that introduction of metal oxide, such as manganese oxide, iron oxides, or aluminum oxide on the surface of activated carbon provide a way for enhancing the adsorption capacity of heavy metals. Heavy metal ions were adsorbed by magnetic separation, surface complexation, and ion exchange mechanisms provided by these metal oxides.

Table 1
BET surface area and pore volume

Samples	BET surface area (m^2/g)	Total pore volume (mL/g)	Micropore volume (mL/g)	Average pore size (nm)
AC	1,417	0.82	0.42	1.85
AC-Fe-350	1,229	0.66	0.33	2.15
AC-Fe-550	1,363	0.75	0.38	2.20
AC-Fe-750	1,164	0.61	0.34	2.10
AC-Fe-950	1,098	0.47	0.25	1.81
AC-Fe-1150	1,026	0.42	0.21	1.76
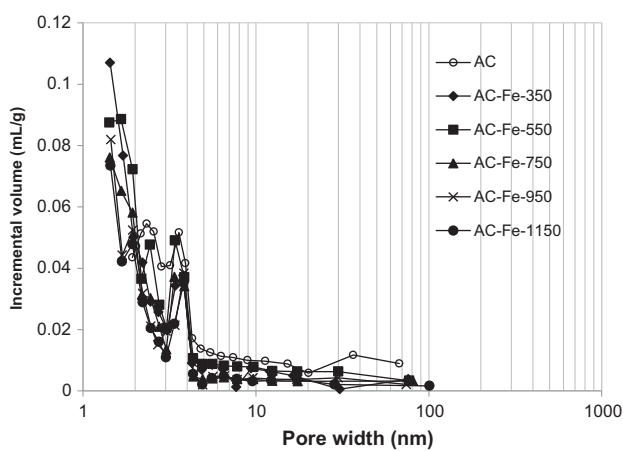
Fig. 5. Pore size distribution of original AC and carbothermally synthesized samples.
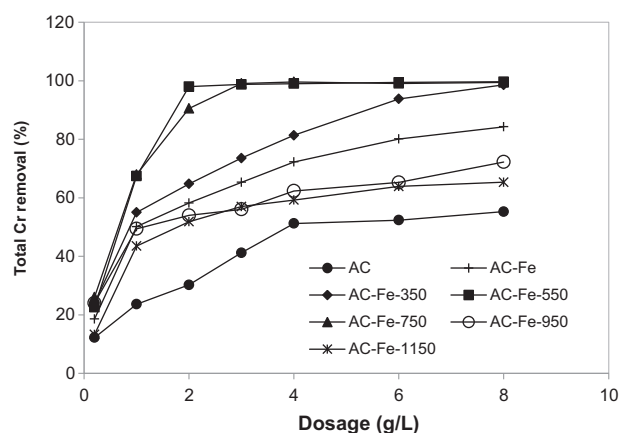
Fig. 6. Effect of dosage on total Cr removal.

The results from this research also revealed that iron oxide could enhance Cr uptake.

Carbothermal reduction could further increase Cr removal. In particular, AC-Fe-350, AC-Fe-550, and AC-Fe-750 all showed higher Cr removal than AC-Fe at the same dosage. The exception resided with

AC-Fe-950 and AC-Fe-1150. Their Cr removals were lower. It seems that thermal treatment at high temperature actually created adverse effects.

In summary, at the same dosage, total Cr removal follows the order of AC-Fe-550 ≈ AC-Fe-750 > AC-Fe-350 > AC-Fe > AC-Fe-950 ≈ AC-Fe-1150 > AC.

3.3. Effect of contact time

Experiments of contact time were conducted to study the kinetics of Cr removal. Fig. 7 shows the change in total Cr removal at different contact times. A rapid initial rise of Cr removal was observed for all samples. Equilibrium was reached within 8 h.

Pseudo-first- and pseudo-second-order models were employed to describe the process of removal.

Pseudo-first-order model:

$$\ln(q_e - q_t) = \ln q_e - k_1 t \tag{2}$$

where q_e and q_t are the amounts of total Cr removed (mg/g) at equilibrium and at time t, respectively, and k_1 is the rate constant (1/h).

Pseudo-second-order model:
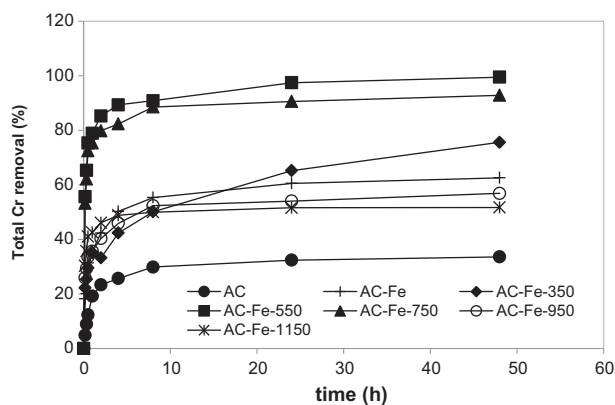
Fig. 7. Effect of contact time on total Cr removal.

Table 2
Kinetic parameters of pseudo-first-order and pseudo-second-order models for Cr(VI) removal

Samples	$q_{e,exp}$[a] (mg/g)	Pseudo-first-order			Pseudo-second-order		
		$q_{e,cal}$[b] (mg/g)	k_1 (1/h)	R^2	$q_{e,cal}$[b] (mg/g)	k_2 g/(mg h)	R^2
AC	6.71	3.94	0.034	0.85	6.83	0.033	0.98
AC-Fe	12.51	6.82	0.069	0.87	12.66	0.098	0.99
AC-Fe-350	15.12	10.18	0.092	0.90	15.24	0.10	0.97
AC-Fe-550	20.15	6.17	0.18	0.68	19.96	0.14	0.98
AC-Fe-750	18.57	5.31	0.12	0.75	18.59	0.18	0.98
AC-Fe-950	11.38	5.00	0.10	0.88	11.67	0.14	0.99
AC-Fe-1150	10.34	2.92	0.12	0.85	10.68	0.15	0.98

[a]Experimental data.
[b]Calculated from model.

$$\frac{t}{q_t} = \frac{1}{k_2 q_e^2} + \frac{t}{q_e} \tag{3}$$

where k_2 is the rate constant of pseudo-second-order reaction (g/(mg h)).

Table 2 lists the kinetic parameters of first- and second-order reactions. It is noted that, in all cases, correlation coefficient (R^2) for pseudo-first-order model is less than 0.90 which is indicative of a bad correlation. In contrast, the application of pseudo-second-order model leads to much better coefficient of around 0.98–0.99. Moreover, the calculated values of q_e are in much better agreement with experiment data. Thus, second-order kinetic model is more suitable to depict the Cr removal suggesting that the process involves chemical reaction mechanism. AC-Fe-550 and AC-Fe-750 manifested the highest Cr removal capacity, with calculated adsorption capacity at equilibrium of 19.96 and 18.59 mg/g. In addition, second-order reaction rates (k_2) were one magnitude higher for carbothermally treated samples compared with AC and AC-Fe. The removal capacities agree well with results from dosage test; carbothermal treatment at extreme high temperature (>950℃) resulted in the loss of removal ability.

3.4. Mechanism of Cr removal

During kinetic study, Change of Cr speciation with the change of time was monitored. Almost no Cr(III) was detected for AC and AC-Fe indicating that Cr removal by these materials is mostly through adsorption and no reduction occurred. In contrast, carbothermal samples all had Cr(III) detected in solution indicating that a portion of initial Cr(VI) was reduced. Petala et al. suggested that iron nanoparticles probably
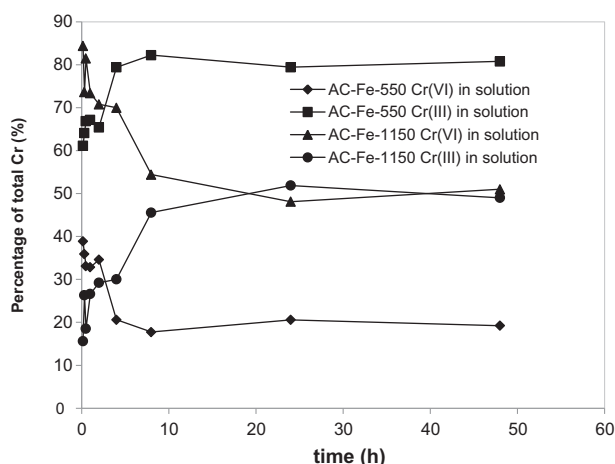
Fig. 8. Cr speciation in aqueous phase for AC-Fe-550 and AC-Fe-1150.

operate as generators of reducing species, e.g. Fe(II) or H/H_2 rather than as direct reducing agent [31].

Fig. 8 is the changes in percentage of Cr(VI) and Cr(III) in total Cr with the change of time for AC-Fe-550 and AC-Fe-1150 in solution as example. As shown in Fig. 7, overall, 97.5 and 52% of the initial Cr was removed after 24 h for AC-Fe-550 and AC-Fe-1150, respectively. A rapid decrease of Cr(VI) was observed during the first 6 h of reaction, while fraction of Cr(III) increased. For AC-Fe-550, Cr(III) accounted for 80% of the residual total Cr in solution after 4 h. This number is 48% for AC-Fe-1150. It appears that AC-Fe-550 showed stronger reduction ability than AC-Fe-1150. This could be due to the differences both in Fe composition and surface properties of activated carbon. As shown from XRD, reoxidation of elemental iron was more severe with AC-Fe-1150, which may mean that elemental iron was encapsulated in a thick

layer of ion oxides and its reduction ability was not released. In addition, AC-Fe-550 had higher surface area and pore volume than AC-Fe-1100, which may also contribute to its higher Cr(VI) removal and reduction capacity. High surface area means more adsorption sites which could create an environment of enriched Cr(VI) around iron particles, thus may accelerate reduction. Cr(III) became the main Cr form with AC-Fe-550 in aqueous phase, which is considered less toxic than Cr(VI).

Speciation of Cr on solid surface of AC-Fe-550 and AC-Fe-1150 were also investigated. Combining with Cr speciation in solution, around 96% of the initial total Cr was account for. The rest 4–5% may not be extracted by the digestion method.

Fig. 9 is the change in Cr(VI) and Cr(III) content with the change of time on solid phase for AC-Fe-550. If Cr removal was dominated by adsorption process, Cr(VI) content on solid phase should be stable with time. However, Fig. 9 show that Cr(VI) was stable around 95% in the first 1 h and dropped drastically to 58–62% from 1 to 8 h. This contradiction proved that the removal pathway was partly attributed to reduction. It is believed that Cr(VI) was fast reduced to Cr(III) by elemental iron and part of the Cr(III) may diffuse back to solution which resulted in an increase in Cr(III) in aqueous phase. Burks et al. reported that Cr(III) could also be co-precipitated with Fe^{3+} onto solid surface [32]. As the reduction and co-precipitation progressed, the surface was gradually covered by excess reaction products, which might act as physical barrier preventing further transport of electron. This may explain why Cr removal leveled off at longer contact time as shown in Fig. 7. Cr(VI) and Cr(III) content on solid were stable after 10 h of contact with about

52% being Cr(VI) and the rest Cr(III) for AC-Fe-550. Cr speciation for AC-Fe-1150 surface followed the same trend with about 75–82% of the Cr(VI) adsorbed on solid surface instead of being reduced to Cr(III). Cr speciation on solid and aqueous phase both showed lesser reduction of Cr(VI) by AC-Fe-1150.

In summary, with carbothermally synthesized samples, besides adsorption, a significant portion of the initial Cr(VI) was reduced.

4. Conclusions

Carbothermal synthesis of activated carbon supported NZVI was carried out in this research. TEM images, XRD patterns, FTIR spectra, BET surface area, and pore volume analysis of synthesized materials revealed that carbothermal temperature played a significant role. It affected the morphology, size of the nanoparticles, extent of dispersion, crystalline structure, surface functional groups, surface area, and pore structure. When temperature was low (about 350℃), iron oxides may still be the main species. Reduction of iron oxides to elemental iron progressed with the increase in temperature. However, extreme temperature as high as 1,150℃ probably results in a surface that is reactive in air and iron oxides reappeared. In addition, dispersion of nanoparticles on activated carbon increased as the temperature increased. Besides, effect of activation and sintering resulted in difference in pore volume and surface area. Activation was strongest at temperature around 550℃ and the resultant materials had the highest pore volume and surface area. Studies on Cr removal were conducted to test the reactivity. At the same dosage, total Cr removal followed the order of AC-Fe-550 ≈ AC-Fe-750 > AC-Fe-350 > AC-Fe > AC-Fe-950 ≈ AC-Fe-1150 > AC. Temperature is significant in determining the reactivity. Also, Cr removal followed the assumption of pseudo-second-order reaction well with correlation coefficient greater than 0.97.

Overall, combining results from characterization and reactivity, temperatures between 550 and 750℃ seem optimum based on the formation of elemental of iron, chromate removal capability, and removal rate.
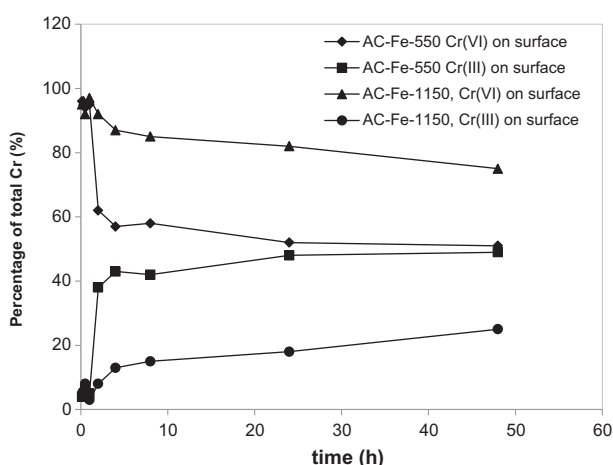
Fig. 9. Cr speciation on solid surface for AC-Fe-550 and AC-Fe-1150.

References

[1] K.D. Grieger, A. Fjordboge, N.B. Hartmann, E. Eriksson, P.L. Bjerg, A. Baun, Environmental benefits and risks of zero-valent iron nanoparticles (nZVI) for *in situ* remediation: Risk mitigation or trade-off? J. Contam. Hydrol. 118 (2010) 165–183.

[2] F.L. Fu, D.D. Dionysiou, H. Liu, The use of zero-valent iron for groundwater remediation and wastewater treatment: A review, J. Hazard. Mater. 267 (2014) 194–205.

[3] Q.J. Rasheed, K. Pandian, K. Muthukumar, Treatment of petroleum refinery wastewater by ultrasound-dispersed nanoscale zero-valent iron particles, Ultrason. Sonochem. 18 (2011) 1138–1142.

[4] T. Raychoudhury, N. Tufenkji, S. Ghoshal, Aggregation and deposition kinetics of carboxymethyl cellulose-modified zero-valent iron nanoparticles in porous media, Water Res. 46 (2012) 1735–1744.

[5] A.I.A. Chowdhury, D.M. O'Carroll, Y.Q. Xu, B.E. Sleep, Electrophoresis enhanced transport of nano-scale zero valent iron, Adv. Water Res. 40 (2012) 71–82.

[6] N.D. Berge, C.A. Ramsburg, Oil-in-water emulsions for encapsulated delivery of reactive iron particles, Environ. Sci. Technol. 43 (2009) 5060–5066.

[7] F. He, D.Y. Zhao, C. Paul, Field assessment of carboxymethyl cellulose stabilized iron nanoparticles for *in situ* destruction of chlorinated solvents in source zones, Water Res. 44 (2010) 2360–2370.

[8] T. Phenrat, H.J. Kim, F. Fagerlund, T. Illangasekare, R.D. Tilton, G.V. Lowry, Particle size distribution, concentration, and magnetic attraction affect transport of polymer-modified Fe-0 nanoparticles in sand columns, Environ. Sci. Technol. 43 (2009) 5079–5085.

[9] Y.H. Lin, H.H. Tseng, M.Y. Wey, M.D. Lin, Characteristics of two types of stabilized nano zero-valent iron and transport in porous media, Sci. Total Environ. 408 (2010) 2260–2267.

[10] T. Raychoudhury, N. Tufenkji, S. Ghoshal, Straining of polyelectrolyte-stabilized nanoscale zero valent iron particles during transport through granular porous media, Water Res. 50 (2014) 80–89.

[11] X. Qiu, Z. Fang, B. Liang, F. Gu, Z. Xu, Degradation of decabromodiphenyl ether by nano zero-valent iron immobilized in mesoporous silica microspheres, J. Hazard. Mater. 193 (2011) 70–81.

[12] H.Y. Shu, M.C. Chang, C.C. Chen, P.E. Chen, Using resin supported nano zero-valent iron particles for decoloration of Acid Blue 113 azo dye solution, J. Hazard. Mater. 184 (2010) 499–505.

[13] S. Bhowmick, S. Chakraborty, P. Mondal, W. Van Renterghem, S. Van den Berghe, G. Roman-Ross, D. Chatterjee, M. Iglesias, Montmorillonite-supported nanoscale zero-valent iron for removal of arsenic from aqueous solution: Kinetics and mechanism, Chem. Eng. J. 243 (2014) 14–23.

[14] X.S. Lv, J. Xu, G.M. Jiang, X.H. Xu, Removal of chromium(VI) from wastewater by nanoscale zero-valent iron particles supported on multiwalled carbon nanotubes, Chemosphere 85 (2011) 1204–1209.

[15] J. Xu, X.S. Lv, J.D. Li, Y.Y. Li, L. Shen, H.Y. Zhou, X.H. Xu, Simultaneous adsorption and dechlorination of 2,4-dichlorophenol by Pd/Fe nanoparticles with multi-walled carbon nanotube support, J. Hazard. Mater. 225–226 (2012) 36–45.

[16] S.A. Kim, S. Kamala-Kannan, K.J. Lee, Y.J. Park, P.J. Shea, W.H. Lee, H.M. Kim, B.T. Oh, Removal of Pb(II) from aqueous solution by a zeolite–nanoscale zero-valent iron composite, Chem. Eng. J. 217 (2013) 54–60.

[17] Y.J. Oh, H. Song, W.S. Shin, S.J. Choi, Y.H. Kim, Effect of amorphous silica and silica sand on removal of chromium(VI) by zero-valent iron, Chemosphere 66 (2007) 858–865.

[18] Y.L. Zhang, Y.M. Li, J.F. Li, G.D. Sheng, Y. Zhang, X.M. Zheng, Enhanced Cr(VI) removal by using the mixture of pillared bentonite and zero-valent iron, Chem. Eng. J. 185–186 (2012) 243–249.

[19] F.C.C. Moura, G.C. Oliveira, M.H. Araujo, J.D. Ardisson, W.A.D. Macedo, R.M. Lago, Formation of highly reactive species at the interface Fe degrees-iron oxides particles by mechanical alloying and thermal treatment: Potential application in environmental remediation processes, Chem. Lett. 34 (2005) 1172–1173.

[20] L.B. Hoch, E.J. Mack, B.W. Hydutsky, J.M. Hershman, I.M. Skluzacek, T.E. Mallouk, Carbothermal synthesis of carbon-supported nanoscale zero-valent iron particles for the remediation of hexavalent chromium, Environ. Sci. Technol. 42 (2008) 2600–2605.

[21] J. Zhan, I. Kolesnichenko, B. Sunkara, J. He, G.L. McPherson, G. Piringer, V.T. John, Multifunctional iron−carbon nanocomposites through an aerosol-based process for the *in situ* remediation of chlorinated hydrocarbons, Environ. Sci. Technol. 45 (2011) 1949–1954.

[22] M.C. Pereira, F.S. Coelho, C.C. Nascentes, J.D. Fabris, M.H. Araujo, K. Sapag, L.C.A. Oliveira, R.M. Lago, Use of activated carbon as a reactive support to produce highly active-regenerable Fe-based reduction system for environmental remediation, Chemosphere 81 (2010) 7–12.

[23] S. Bleyl, F.D. Kopinke, K. Mackenzie, Carbo-Iron®—Synthesis and stabilization of Fe(0)-doped colloidal activated carbon for *in situ* groundwater treatment, Chem. Eng. J. 191 (2012) 588–595.

[24] K. Mackenzie, S. Bleyl, A. Georgi, F.D. Kopinke, Carbo-iron—An Fe/AC composite—As alternative to nano-iron for groundwater treatment, Water Res. 46 (2012) 3817–3826.

[25] Y.H. Hwang, D.G. Kim, H.S. Shin, Effects of synthesis conditions on the characteristics and reactivity of nano scale zero valent iron, Appl. Catal., B 105 (2011) 144–150.

[26] H.Q. Sun, G.L. Zhou, S.Z. Liu, H.M. Ang, M.O. Tade, S.B. Wang, Nano-Fe-0 encapsulated in microcarbon spheres: Synthesis, characterization, and environmental applications, Acs. Appl. Mater. Inter. 4 (2012) 6235–6241.

[27] Y. Zeng, H. Woo, G. Lee, J. Park, Adsorption of Cr(VI) on hexadecylpyridinium bromide (HDPB) modified natural zeolites, Microporous Mesoporous Mater. 130 (2010) 83–91.

[28] V.S. De Portilla, The nature of hydrogen bonds and water in legrandite by IR spectroscopy, Am. Mineral. 61 (1976) 95–99.

[29] Y.F. Su, Y.L. Cheng, Y.H. Shih, Removal of trichloroethylene by zerovalent iron/activated carbon derived

from agricultural wastes, J. Environ. Manage. 129 (2013) 361–366.

[30] C. Luo, Z. Tian, B. Yang, L. Zhang, S.Q. Yan, Manganese dioxide/iron oxide/acid oxidized multi-walled carbon nanotube magnetic nanocomposite for enhanced hexavalent chromium removal, Chem. Eng. J. 234 (2013) 256–265.

[31] E. Petala, K. Dimos, A. Douvalis, T. Bakas, J. Tucek, R. Zboril, M.A. Karakassides, Nanoscale zero-valent iron supported on mesoporous silica: Characterization and reactivity for Cr(VI) removal from aqueous solution, J. Hazard. Mater. 261 (2013) 295–306.

[32] T. Burks, M. Avila, F. Akhtar, M. Göthelid, P.C. Lansåker, M.S. Toprak, M. Muhammed, A. Uheida, Studies on the adsorption of chromium(VI) onto 3-Mercaptopropionic acid coated superparamagnetic iron oxide nanoparticles, J. Colloid Interface Sci. 425 (2014) 36–43.